

Identification of the phosphorus-doping defect in MgS as a potential qubit

Jijun Huang(黄及军) and Xueling Lei(雷雪玲)

Citation: Chin. Phys. B, 2022, 31 (**10**): 106102. DOI: 10.1088/1674-1056/ac7dbc
Journal homepage: http://cpb.iphy.ac.cn; http://iopscience.iop.org/cpb

What follows is a list of articles you may be interested in

Lattice damage in InGaN induced by swift heavy ion irradiation

Ning Liu(刘宁), Li-Min Zhang(张利民), Xue-Ting Liu(刘雪婷), Shuo Zhang(张硕), Tie-Shan Wang(王铁山), and Hong-Xia Guo(郭红霞)
Chin. Phys. B, 2022, 31 (**10**): 106103. DOI: 10.1088/1674-1056/ac7ccd

Direct visualization of structural defects in 2D semiconductors

Yutuo Guo(郭玉拓), Qinqin Wang(王琴琴), Xiaomei Li(李晓梅), Zheng Wei(魏争), Lu Li(李璐), Yalin Peng(彭雅琳), Wei Yang(杨威), Rong Yang(杨蓉), Dongxia Shi(时东霞), Xuedong Bai(白雪冬), Luojun Du(杜罗军), and Guangyu Zhang(张广宇)
Chin. Phys. B, 2022, 31 (**7**): 076105. DOI: 10.1088/1674-1056/ac6738

First-principles study of stability of point defects and their effects on electronic properties of GaAs/AlGaAs superlattice

Shan Feng(冯山), Ming Jiang(姜明), Qi-Hang Qiu(邱启航), Xiang-Hua Peng(彭祥花), Hai-Yan Xiao(肖海燕), Zi-Jiang Liu(刘子江), Xiao-Tao Zu(祖小涛), and Liang Qiao(乔梁)
Chin. Phys. B, 2022, 31 (**3**): 036104. DOI: 10.1088/1674-1056/ac16cb

Modification of short-range repulsive interactions in ReaxFF reactive force field for Fe-Ni-Al alloy

Huaqiang Chen(陈华强), Lin Lang(稂林), Shuaiyu Yi(易帅玉), Jinlong Du(杜进隆), Guangdong Liu(刘广东), Lixia Liu(刘丽霞), Yufei Wang(王宇飞), Yuehui Wang(王悦辉), Huiqiu Deng(邓辉球), and Engang Fu(付恩刚)
Chin. Phys. B, 2021, 30 (**8**): 086110. DOI: 10.1088/1674-1056/ac0901

Evolution of ion-irradiated point defect concentration by cluster dynamics simulation

Shuaishuai Feng(冯帅帅), Shasha Lv(吕沙沙), Liang Chen(陈良), and Zhengcao Li(李正操)
Chin. Phys. B, 2021, 30 (**5**): 056105. DOI: 10.1088/1674-1056/abf102

RAPID COMMUNICATION

Identification of the phosphorus-doping defect in MgS as a potential qubit

Jijun Huang(黄及军) and Xueling Lei(雷雪玲)†

Department of Physics, Jiangxi Normal University, Nanchang 330022, *China*

(Received 8 April 2022; revised manuscript received 19 May 2022; accepted manuscript online 2 July 2022)

The P_S defect is obtained by replacing one S atom with one P atom in the wide-bandgap semiconductor MgS. Based on first-principles calculations, the formation energy, defect levels, and electronic structure of the P_S defect in different charge states are evaluated. We predict that the neutral P_S^0 and positively charged P_S^{+1} are the plausible qubit candidates for the construction of quantum systems, since they maintain the spin conservation during optical excited transition. The zero-phonon lines at the P_S^0 and P_S^{+1} defects are 0.43 eV and 0.21 eV, respectively, which fall in the infrared band. In addition, the zero-field splitting parameter D of the P_S^{+1} with spin-triplet is 2920 MHz, which is in the range of microwave, showing that the P_S^{+1} defect can be manipulated by microwave. Finally, the principal values of the hyperfine tensor are examined, it is found that they decay exponentially with the distance from the defect site.

Keywords: point defects, MgS semiconductor, qubits, first-principles calculations

PACS: 61.72.J–, 61.72.jn, 61.72.U–, 71.22.+i **DOI:** 10.1088/1674-1056/ac7dbc

1. Introduction

The defects of wide-bandgap semiconductors have attracted extensive attention due to their great potential for applications in quantum sensing,[1,2] information processing,[3,4] and so on. For example, point defects in semiconductors are used as quantum sensors to measure temperature,[5,6] electric field,[7] magnetic field,[8] etc. It is known that the famous negatively charged NV color center and SiV color center in diamond[9–11] have excellent properties, e.g., microwave manipulation,[12] long spin coherence time,[13] and controllable coupling between individual electronic and nuclear spins.[4] However, the preparation process of NV^- color center in diamond is still challenging because of the requirements of high concentration and controllable position.[14–16] Therefore, it is necessary to find other potential qubits to apply in the quantum systems. So far, many candidates have been proposed, such as negatively charged Si vacancy (V_{Si}^-),[17,18] neutral carbon–silicon double vacancy (V_CV_{Si}),[19,20] and negatively charged NV color center ($N_CV_{Si}^-$)[21] in SiC, the neutral $V_{Al}O_N$ in wurtzite AlN,[22] the neutral $V_{Ga}O_N$ in GaN,[23] etc.

MgS is a typical wide-bandgap semiconductor (experimental bandgap: 4.45 eV[24,25]) with diamond like structure, and it has been successfully prepared experimentally. Inspired by the above works, the phosphorus-doping defect (P_S) in MgS as a potential qubit has been systematically investigated using first-principles calculations. The aim of this work is to find a qubit candidate with excellent quantum properties. The formation energy, defect levels, and electronic structure of the P_S defect in different charge states are evaluated. The zero-phonon line (ZPL) and zero field splitting (ZFS) of neutral P_S^0 and positively charged P_S^{+1} are discussed, and the hyperfine tensors are examined. Our calculations suggest that the neutral P_S^0 and positively charged P_S^{+1} are the plausible qubit candidates for the construction of quantum systems.

2. Computational details

All the first-principles calculations in this work have been carried out using the Vienna *ab initio* simulation package (VASP)[26,27] in the framework of the density functional theory (DFT). The interaction between core ions and valence electrons was described by the projector augmented wave (PAW) method[28,29] and the generalized gradient approximation (GGA) parametrized by Perdew–Burke–Ernzerhof (PBE)[30] was used for the exchange–correlation functional. Geometries of the $2\times2\times2$ MgS supercell with one Ps defect in different charge states were fully optimized using a plane wave cutoff of 400 eV without any symmetry restrictions, the energy and force convergence were set to be 1×10^{-5} eV and 0.01 eV·Å^{-1}, respectively. The 0.02 Å^{-1} Monkhorst–Pack k-point density of the supercell was set for Brillouin zone sampling.[31] It is known that the bandgap calculated with PBE usually has been underestimated, and the Heyd–Scuseria–Ernzerhof (HSE06)[32,33] hybrid exchange–correlation functional allows one to solve this problem. Then the HSE06 was afterward chosen to study the electronic structures and optical properties.

In order to describe the stability of the P-doped point defects (denoted as P_S), the defect formation energy was calcu-

†Corresponding author. E-mail: xueling@mail.ustc.edu.cn

© 2022 Chinese Physical Society and IOP Publishing Ltd

lated according to[34]

$$E_{\text{form}}\left[\mathrm{P}_{\mathrm{S}}^{q}\right] = E_{\text{total}}\left[\mathrm{P}_{\mathrm{S}}^{q}\right] - E_{\text{total}}\left[\text{bulk}\right] + \mu_{\mathrm{S}} - \mu_{\mathrm{P}} + q\left(\Delta\varepsilon_{\mathrm{F}} + \varepsilon_{\mathrm{VBM}}^{\text{bulk}} + \Delta V\right), \quad (1)$$

where $E_{\text{total}}\left[\mathrm{P}_{\mathrm{S}}^{q}\right]$ and $E_{\text{total}}\left[\text{bulk}\right]$ are the total energy of the supercell with and without $\mathrm{P_S}$ defect, respectively, and q is the charge state of the system. μ_{S} and μ_{P} are the chemical potentials of S and P atoms. Under S-rich conditions, μ_{S} is calculated from bulk sulfur and $\mu_{\mathrm{Mg}} = \mu_{\mathrm{MgS}} - \mu_{\mathrm{S}}$. Under Mg-rich conditions, μ_{Mg} is calculated from bulk Mg and $\mu_{\mathrm{S}} = \mu_{\mathrm{MgS}} - \mu_{\mathrm{Mg}}$. The μ_{MgS} is the chemical potential of one MgS unit in MgS crystal. $\Delta\varepsilon_{\mathrm{F}}$ represents the Fermi level, and the value ranges from 0 to the gap of a perfect MgS crystal. $\varepsilon_{\mathrm{VBM}}^{\text{bulk}}$ is the maximum value of the valence band of a perfect MgS crystal. ΔV is the correction term, which is used to balance the electrostatic potential between perfect and defective MgS supercells.

3. Results and discussion

3.1. Structural and electronic properties of the $\mathrm{P_S}$ point defects in MgS

The optimized structure parameters and bandgap of MgS primitive cell are listed in Table 1, from which we can see that the lattice parameter of MgS primitive cell is 4.025 Å and the Mg–S bond length is 2.465 Å. The point defect of $\mathrm{P_S}$ has been created by substituting one P atom for one S atom in a $2\times2\times2$ MgS supercell. Since each S atom in MgS is equivalent, there is only one type of the $\mathrm{P_S}$ point defect. The optimized geometry of the neutral $\mathrm{P_S}$ point defect along with the electronic structures is shown in Fig. 1. After optimization, the $\mathrm{P_S}$ point defect has C_{3v} symmetry. As shown in Fig. 1(a), the distances between P atom and the four nearest Mg atoms are 2.51 Å, 2.51 Å, 2.51 Å, and 2.68 Å, respectively. Comparing with the distance of S–Mg in the perfect MgS crystal (2.47 Å), all the distances of P–Mg have been stretched. $\mathrm{Mg_4}$ and P atoms are on the axis of symmetry. The distance of $\mathrm{Mg_4}$–Mg_i (i = 1, 2, 3) is 4.10 Å, and the distance between Mg_i (i = 1, 2, 3) is 4.20 Å. According to formula (1), the calculated formation energy of the neutral $\mathrm{P_S}$ point defect ($q = 0$) is 4.10 eV and 0.54 eV under S-rich and Mg-rich conditions, respectively, indicating that the $\mathrm{P_S}$ point defect is easy to form in the case of Mg-rich.

Table 1. The structure parameters and bandgap of the MgS primitive cell.

$a = b = c$	$\alpha = \beta = \gamma$	$d_{\mathrm{Mg-S}}$	HSE bandgap	Exp. bandgap[24]
4.025 Å	60°	2.465 Å	4.44 eV	4.45 eV

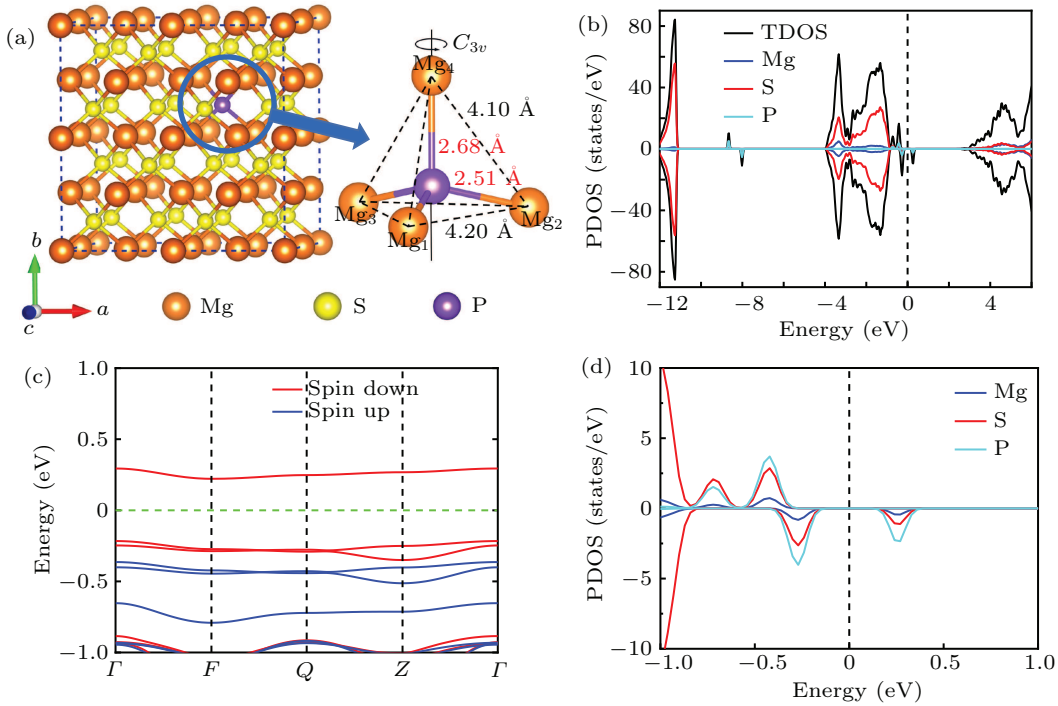


Fig. 1. The schematic diagram of the $\mathrm{P_S}$ point defect in a $2\times2\times2$ MgS supercell and the local structure of the $\mathrm{P_S}$ point defect (a) and corresponding projected density of states (PDOS) (b), the amplified PDOS (c) and band structure (d) with an energy range of −1.00 eV to 1.00 eV.

Now, we turn to examine the electronic structures of the $\mathrm{P_S}$ point defect. The electronic structures calculated from $4\times4\times4$ supercell with 512 atoms are presented in Fig. S1 in the supplementary material, from which the characteristics of electronic structures are the same as those of 64 atoms supercell. As shown in Fig. 1(b), the spin polarization projected density of states (PDOS) of the $\mathrm{P_S}$ point defect shows that there are six defect states due to introduction of the impurity P atom. Of those defect states, two occupied defect states lie very deep in the valence band, one is spin-up electronic state at

−8.67 eV, the other is spin-down electronic state at −8.02 eV, so the two states play no important role in the excitation or ionization processes. Four defect states are located in the bandgap of the host material MgS. Of those, three defect states are occupied electronic states and the remaining one is the unoccupied electronic state. Further observation, it is found that the peak of two occupied states close to the Fermi level is about twice as high as that of one occupied state near the valence band maximum (VBM), indicating that the two occupied defect states are double degenerate states. To illustrate this, we further examine the band structure near the Fermi level. Figure 1(c) shows the amplified band structure with an energy range of −1.00 eV to 1.00 eV. We note that there are indeed two double degenerate defect levels below the Fermi level, one is spin up and the other is spin down. And there are two singlet defect levels in the gap of the MgS, one is close to the VBM and the other one is above the Fermi level, this is consistent with the results in Fig. 1(b). Combined with the PDOS and the amplified band structure, it is easy to know that there are five defect energy levels occupied by electrons, and two of them are double degenerate defect energy levels. As a result, the defect energy levels have been occupied by seven electrons. However, the impurity P atom has a total of five valence electrons, so where do the extra two electrons that occupy the defect energy levels come from? To understand this question, we further draw the amplified PDOS near the Fermi level, as shown in Fig. 1(d), from which we can see that the occupied electronic states in the gap are mainly from the contributions of the valence electrons of P atom and S atom, and slightly from the contributions of Mg atom. Therefore, the defect energy levels are mainly occupied by five valence electrons of P atom and two valence electrons of S atom.

To confirm the above results, we further plotted the schematic diagram of the defect energy level sequence and the corresponding partial charge densities, as shown in Fig. 2. According to the molecular orbitals (MOs) theory in the system with C_{3v} symmetry,[35] there are two non-degenerate MOs $a_1(1)$ and $a_1(2)$ in the one-dimensional irreducible representation (IR) of A_1 space and two degenerate MOs e_x and e_y in the two-dimensional IR of E space. Correspondingly, there are two non-degenerate levels E_1 and E_2, and two degenerate levels E_x and E_y, i.e., the E_1, E_2 and E_{xy} levels. Based on the analysis of electronic structures, the defect energy levels of the P_S point defect from high to low are as follows: $E_1^{\downarrow}$, $E_{xy}^{\downarrow}$, $E_{xy}^{\uparrow}$, $E_1^{\uparrow}$, $E_2^{\downarrow}$, $E_2^{\uparrow}$, where E_{xy} represents double degenerate defect levels. According to Fig. 2(a), the defect energy levels are occupied by seven electrons. Specifically, the E_2 and E_{xy} levels are fully occupied by six electrons, and the E_1 levels is half occupied (spin up) by one electron. Therefore, the net spin of the system is $S = 1/2$ and then the system is spin-doublet. As seen in Fig. 2(b), the P atom and its nearest S atoms make the largest contribution to the charge density of the E_1 and E_{xy} levels, while the charge density of the E_2 level is only localized on the P atom, showing that the E_2 is occupied only by the valence electrons of P atom. Considering the distribution shape of the electron density, it can be concluded that the 3p electrons of P atom and S atom occupy the E_1 and E_{xy} levels, and 3s electrons of P atom occupy the E_2 level. Furthermore, we also observe that the area of charge density distributed on E_{xy} is almost twice as large as that distributed on E_1, indicating that the E_{xy} level is a double degenerate energy level. These results are in good agreement with the aforementioned electronic structure analysis.

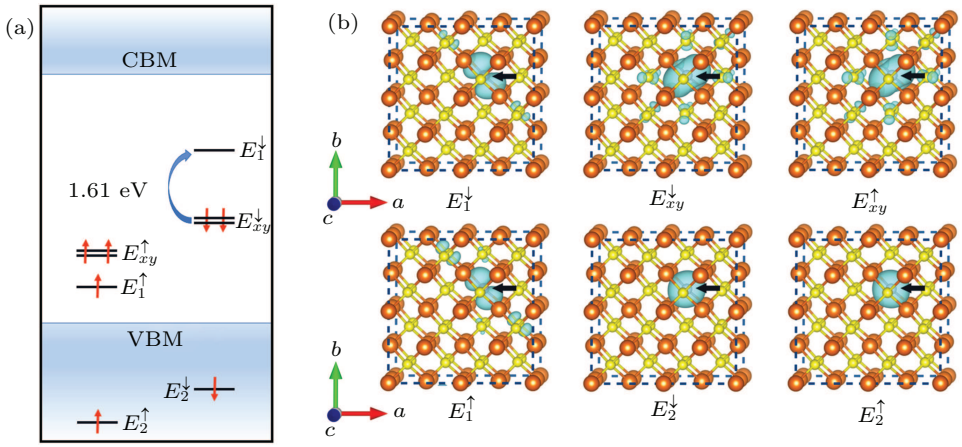


Fig. 2. The schematic diagram of the defect energy levels (a) and the partial charge density of molecular orbitals (b) in the P_S defect in the order of energy from high to low. The isosurface value is 2×10^{-3} e/Å^3. The black arrow indicates the position of the P_S defect.

When the system is optically excited, the electron on the $E_{xy}^{\downarrow}$ level will transition to the $E_1^{\downarrow}$ level. Here, for the sake of convenience, we define the energy difference between the $E_{xy}^{\downarrow}$ level and the $E_1^{\downarrow}$ level as ΔE, between the $E_{xy}^{\downarrow}$ level and the VBM as ΔE_V, and between the $E_1^{\downarrow}$ level and the conduction band minimum (CBM) as ΔE_c. In addition, to avoid the intrinsic underestimation of the bandgap, the HSE06 hybird exchange–correlation functional has been used to calculate the

energy gap. As shown in Table 2, the ΔE is 0.46 eV and 1.61 eV calculated at the PBE and HSE06 level, respectively. The HSE06 energy gap is smaller than 1.8 eV of the NV^{-1} color center in diamond,[36] indicating that it takes less energy to excite electrons in the P_S point defect in MgS. At the same time, we also note that ΔE_V is 0.68 eV at the HSE06 level, which is smaller than the ΔE, then the electronic states of the host material may interfere with the electronic transition.[14]

Table 2. Energies (in eV) of the P_S^0 defect levels ($E_1^{\downarrow}$ and $E_{xy}^{\downarrow}$), CBM, VBM, and the energy gap (ΔE, ΔE_c and ΔE_V) calculated by HSE06 and PBE, respectively. The energies of $E_1^{\downarrow}$, $E_{xy}^{\downarrow}$, CBM and VBM are relative to the Fermi level, and the Fermi level is set to be zero.

	$E_1^{\downarrow}$	$E_{xy}^{\downarrow}$	CBM	VBM	ΔE	ΔE_c	ΔE_V
PBE	0.23	–0.23	2.50	–0.88	0.46	2.27	0.65
HSE06	1.17	–0. 44	3.35	–1.12	1.61	2.18	0.68

3.2. Different charge states of the P_S point defects in MgS

As aforementioned, the total spin of the neutral P_S point defect is $S = 1/2$ with one unpaired electron, where S is the spin angular momenta, and then the neutral P_S point defect is spin-doublet. As we know, the triplet qubit with total spin $S = 1$ can be easily manipulated by microwave (MW), so the properties of the P_S point defect in different charge states have been investigated to find easily manipulated triplet qubit. First of all, the energetic stability of the P_S point defects in different charge states was evaluated using the formation energy calculated via formula (1). Figure 3 shows the formation energy of the P_S point defects in the charge state q ($q = -1$, 1, 2) as a function of the Fermi level, where each line represents the formation energy for a specific charge state, and the slope represents the charge state of the system. Obviously, the most stable charge state is affected by the position of the Fermi level, e.g., the solid black lines represent the most stable charge state of the P_S defect with the lowest formation energies corresponding to different Fermi levels. The neutral P_S point defect is stable for $\varepsilon_F = 1.96$–2.60 eV. With the Fermi level varying from the VBM to CBM, the most stable charge state of the P_S point defect exhibits P_S^{+2}, P_S^{+1}, P_S^0 and P_S^{-1}, with transition of $+2/+1$, $+1/0$ and $0/-1$. The values of the corresponding charge transition level are 1.51 eV, 1.96 eV and 2.60 eV, respectively.

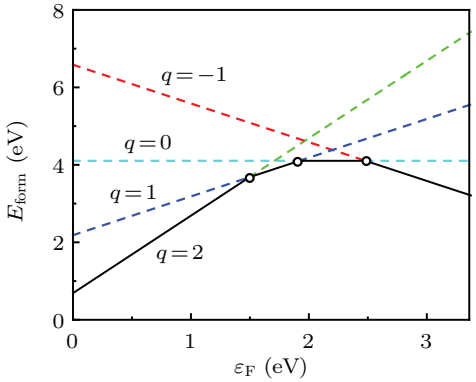


Fig. 3. Formation energies (E_{form}) of the P_S point defect in different charge states as a function of Fermi level (ε_F), the slope represents the charge state q.

Then the basic electronic properties of the P_S point defects in different charge states were calculated and shown in Fig. 4.

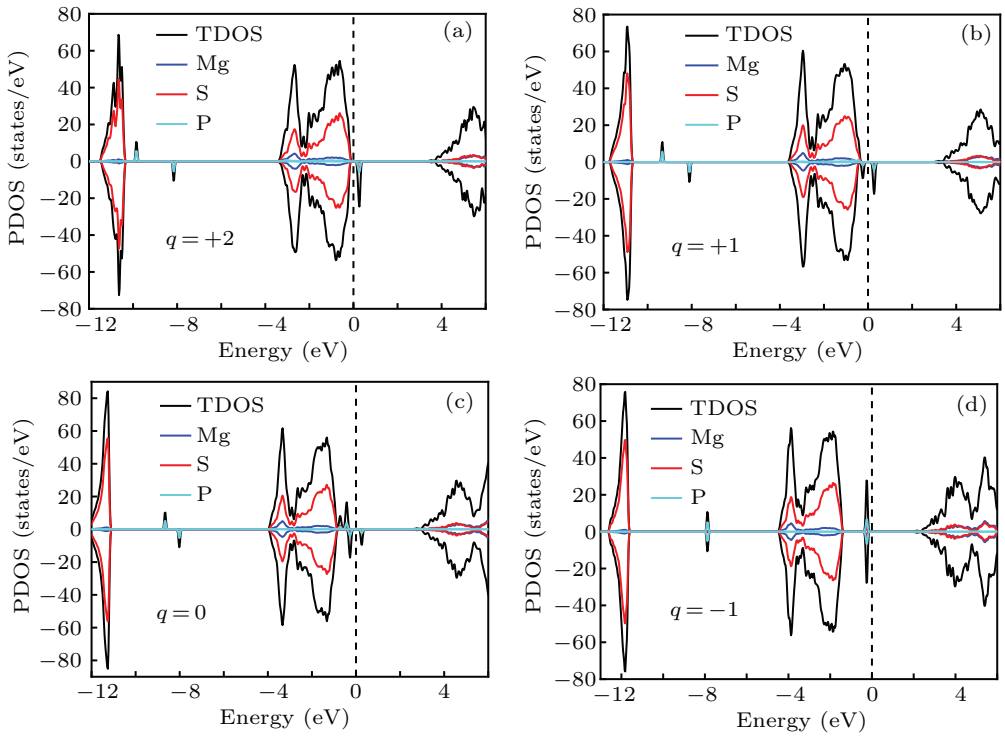


Fig. 4. The projected density of states (PDOS) of the P_S point defect in different charge states.

In the $q = +1$ charge state, an electron is ionized out of the $E_{xy}^{\downarrow}$ level, and thus the $E_{xy}^{\downarrow}$ level is only occupied by one unpaired electron, arising the triplet ground state with two net spins. Accordingly, the total spin angular momenta $S = 1$. Comparing to the $q = 0$ charge state, the PDOS of the P_S^{+1} point defect shows that the spin down unoccupied states increase, whereas the spin down occupied states decrease, and they are close to the VBM of the MgS. Moreover, we noted that the spin up occupied states move into the valence band of the MgS. In this case, an occupied electron can be excited from the $E_{xy}^{\downarrow}$ level into the $E_1^{\downarrow}$ level obeying the spin conservation, and the energy gap between the occupied $E_{xy}^{\downarrow}$ level and the unoccupied $E_1^{\downarrow}$ level to be overcome is 1.49 eV calculated at the HSE06 level, as listed in Table 3. When $q = +2$, the remaining one electron is ionized from the $E_{xy}^{\downarrow}$ level, both the $E_{xy}^{\downarrow}$ level and the $E_1^{\downarrow}$ level are unoccupied levels, resulting in spin-quartet due to its three net spins, and then $S = 3/2$. The PDOS of the P_S^{+2} shows a strong spin down unoccupied peak, and the spin down occupied peak in the $q = +1$ charge state has vanished in the $q = +2$ charge state. The strong spin down peak indicates that it is a three-fold degenerate state. Contrary to the positive charge states, in the $q = -1$ charge state, an extra electron is added into the P_S^0 defect and occupied the $E_1^{\downarrow}$ level. As a result, all the defect levels are fully occupied by electrons, then the spin-up electronic states equal to the spin-down electronic states in energy, so the spin polarization disappears in the PDOS of the P_S^{-1} defect.

Table 3. Energies (in eV) of the P_S^{+1} point defect levels ($E_1^{\downarrow}$ and $E_{xy}^{\downarrow}$), CBM, VBM, and the energy gap (ΔE, ΔE_c and ΔE_V) calculated by HSE06 and PBE, respectively. The energies of $E_1^{\downarrow}$, $E_{xy}^{\downarrow}$, CBM and VBM are relative to the Fermi level, and the Fermi level is set to be zero.

	$E_1^{\downarrow}$	$E_{xy}^{\downarrow}$	CBM	VBM	ΔE	ΔE_C	ΔE_V
PBE	0.29	0.20	2.98	0.50	0.49	2.69	0.30
HSE06	1.27	0.22	4.10	0.41	1.49	2.83	0.19

From the above analysis, the charge state with $q = +1$ and the neutral state may satisfy the requirements of qubit for the realization of optical transition.[14] However, the disadvantage of the P_S^{+1} point defect is that the occupied defect level, i.e. the $E_{xy}^{\downarrow}$ level, is very close to the VBM of the MgS (energy gap: 0.19 eV), which may also introduce the electronic states of the host material to the optical transition.

3.3. Optical properties of the P_S^0 and P_S^{+1} point defects in MgS

For a promising qubit candidate, a very important aspect that determines the quality of a qubit/spin-photon interface is its optical properties. On the one hand, zero-phonon line (ZPL) transition energy determines how feasible it is to integrate and scale the system, e.g., it is access to telecom bands possible directly or via quantum frequency conversion, do convenient laser sources exist, etc. On the other hand, the strength of the phonon sideband determines and limits the rate of coherently emitted photons for optical remote entanglement schemes. The coordinate configuration diagram not only provides some reference for optical detection of magnetic resonance (ODMR), but also enables one to clearly describe the electron–phonon interaction in the system. Therefore, the schematic diagram of the configuration coordinate in the P_S point defect during absorption and emission of photons is drawn in Fig. 5, and the values of an optical absorption/emission in various charge states were calculated and summarized in Table 4. With the transition of an electron from the $E_{xy}^{\downarrow}$ level to the $E_1^{\downarrow}$ level, the system changes from the ground state to excited state. As shown in Fig. 5, two curves represent the potential energy of the ground state and the excited state, respectively. It is believed that the crystal structure maintains the ground state configuration in the process of absorbing photons, since the electron excitation takes a very short time compared to the lattice relaxation. As a result, the energy absorbed during the excitation process is 0.68 eV and 0.42 eV for the P_S^0 and P_S^{+1} point defect, respectively, represented by the red arrow. Similarly, the crystal structure maintains the excited state configuration in the course of the emitting photons, since the electron de-excitation takes a very short time compared to the lattice relaxation, then the energy emitted upon the electron de-excitation is 0.27 eV and 0.09 eV for the P_S^0 and P_S^{+1} point defect, respectively, represented by the blue arrow. In addition, the ZPL is the energy difference between the energy of the optimized excited state and that of the optimized ground state, represented by the red arrow. Table 4 shows that the ZPLs of the P_S^0 and P_S^{+1} calculated at the HSE06 level are 0.43 eV and 0.21 eV, respectively. The corresponding wavelengths are 2883.7 nm and 5904.7 nm, respectively, which belong to the infrared band. In the latter case, it may result in sharp transition in the luminescence if it becomes an allowed process. We expect that these ZPLs will be confirmed by photoluminescence (PL) measurements in the future. These ZPLs are much smaller than 1.95 eV for the NV color centers in diamond[14] and 1.09 eV for the $N_C V_{Si}^{-1}$ centers in 4H-SiC,[14] but is comparable with the 0.575 eV for the $Ni_{Ga}V_N^0$ center in c-GaN,[35] which means that the optical excitation can be easily achieved at lower energy for the P_S^0 and P_S^{+1} point defects. At the same time, the Stokes shift and anti-Stokes shift are also calculated and listed in Table 4, it can be seen that the Stokes shift and anti-Stokes shift are 0.25 eV and 0.16 eV for the P_S^0 point defect, and 0.21 eV and 0.12 eV for the P_S^{+1} point defect. The lower values of ΔS and ΔAS mean the smaller lattice relaxation.

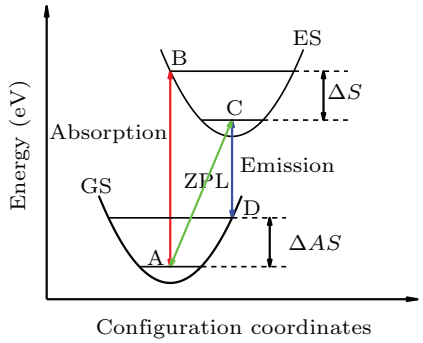


Fig. 5. The schematic diagram of the configuration coordinate of P_S' ground state and excited state. The red and blue arrows represent vertical absorption and vertical emission, respectively, and the green arrow is the zero-phonon line (ZPL). ΔS and ΔAS stand for Stokes shift and anti-Stokes shift, respectively.

Table 4. The zero-phonon lines (in eV) of the P_S point defect in various charge states calculated at the HSE06 level.

	Vertical absorption	Vertical emission	ZPL	ΔS	ΔAS
P_S^0	0.68	0.27	0.43	0.25	0.16
P_S^{+1}	0.42	0.09	0.21	0.21	0.12

In addition, the zero-field splitting tensor (ZFST) of the P_S^{+1} point defect with spin-triplet has been calculated to estimate whether the P_S^{+1} defect can be manipulated by microwave. ZFS is a splitting between the degenerate electron spin sublevels for the system of $S \geq 1$ without an external electric field, which is caused by the electron spin–spin dipole interaction. ZFS has two parameters in the eigenvalue framework, one is axial ZFS parameter D, the other is transverse ZFS parameter E, which are expressed by the diagonal elements of the tensor as[37]

$$D = \frac{3}{2}D_{zz}, \tag{2}$$

$$E = \frac{D_{yy} - D_{xx}}{2}. \tag{3}$$

As a result, $D = 2920$ MHz and $E = -265$ MHz. The value of D is obviously in the range of MW, and in fair agreement with the theoretical data 2980 MHz of the V_BO_N center in c-BN crystal.[16] However, the value of E is ten orders of magnitude smaller than D. We note that the E is not zero, perhaps because the P_S^{+1} point defect is not strict C_{3v} symmetric. We expect that our D can be confirmed by the optically detected magnetic resonance (ODMR) in the future, which is considered to be the core parameter for preparing superposition states in the quantum manipulation process.

3.4. Hyperfine parameters of the P_S^0 and P_S^{+1} point defects in MgS

The hyperfine tensor reflects the interaction between nuclear spin and electron spin.[38] As we know, although the nuclear spins of ^{24}Mg and ^{32}S are zero, the ^{25}Mg (with natural abundance of 10.11%), ^{33}S (0.75%) and ^{31}P (100%) have nonzero nuclear spins of 5/2, 3/2, and 1/2, respectively. Therefore, the hyperfine tensors have been calculated in this work, which are expressed as

$$H_{\text{hyp}} = \sum S_i A_{ij} I_j, \tag{4}$$

where S_i is the electronic spin of the ith electron, I_j is the nuclear spin of the jth nucleus, and A_{ij} is the hyperfine tensor. The hyperfine tensors of different elements with different sites show various results, which is useful for independent manipulation of various nuclear spins. Tables S1 and S2 in the supplementary material list the calculated leading values of the diagonalized hyperfine tensors of the P_S^0 point defect and the P_S^{+1} point defect in MgS, where only the nearest neighbors and the next nearest neighbors atoms as shown in Fig. 6(a) are considered, since the other hyperfine tensors of remote atoms are quite small and can be ignored. According to our calculations, the hyperfine tensors have some common features: the principal values of the hyperfine tensor are the largest on the P atom, and decrease rapidly as the distance from the P atom increases. In addition, the values of A_{xx} are equal to those of A_{yy} for the P atom and Mg_4 atom, which is attributed to the positions of the P and Mg_4 atom on the C_{3v} symmetry axis. We expect that our calculated hyperfine tensors will be compared with the experimental values measured using the appropriate techniques such as electron paramagnetic resonance (EPR) or nuclear magnetic resonance (NMR) in the future.

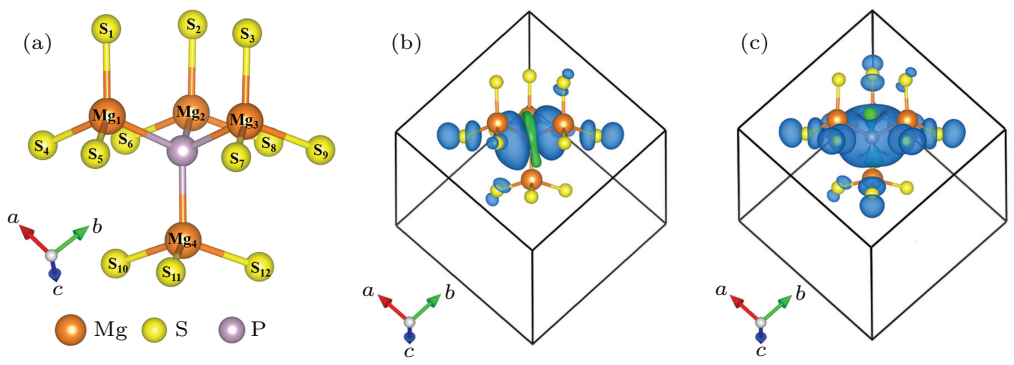


Fig. 6. Schematic diagram of the local structure (a), the spin difference charge density of the P_S^0 point defect (b) and the P_S^{+1} point defect (c) in MgS. We only show the atoms up to the second neighbors from the P atom, the isosurface value is 5×10^{-4} e/Å^3 for the spin difference charge density. The blue and green represent positive and negative, respectively.

Figure 6 shows the schematic diagram of the local structure and the spin difference charge density of the P_S^0 point defect and the P_S^{+1} point defect in MgS, respectively, where only the atoms and the spin difference charge density of the nearest neighbors and the next nearest neighbors of the defect are shown. It can be seen that the spin difference charge density is highly localized at the center of the defect, and dramatically decreases with the distance from the defect center increasing, which is consistent with the findings of the calculated hyperfine tensors.

4. Summary and conclusions

In summary, the P_S point defects in MgS in different charge states have been systematically studied in this paper. The formation energy reveals that the stable structure in various charge states can easily exist in the appropriate Fermi level range. A thorough analysis of the electronic structures evidences that the P_S^0 and P_S^{+1} point defects have spin-doublet and spin-triplet state in the ground state, respectively, and can be maintained during the optically excited transition, which is a pivotal characteristic of the structure as a qubit. The P_S^0 and P_S^{+1} point defects can exist stably in the Fermi energy range of 1.96–2.60 eV and 1.51–1.96 eV, respectively. Based on the accurate HSE06 calculations, the ZPLs of the P_S^0 and the P_S^{+1} are 0.43 eV and 0.21 eV, respectively, corresponding to the infrared band. Besides, the energies of ΔS and ΔAS shifts are 0.25 eV and 0.16 eV for the P_S^0 point defect, 0.21 eV and 0.12 eV for the P_S^{+1} point defect. These values are of great importance for the ODMR applications. In addition, the calculated axial ZFS parameter D and the transverse ZFS parameter E of the P_S^{+1} point defect are 2920 MHz and -265 MHz, respectively. Finally, it has been found that the principal values of the hyperfine tensor decay exponentially with the distance from the defect site.

Acknowledgements

Project supported by the National Natural Science Foundation of China (Grant No. 12164020) and the Natural Science Foundation of Jiangxi Province, China (Grant No. 20202BAB201012). We gratefully acknowledge Hefei Advanced Computing Center for computational support.

References

[1] Degen C L, Reinhard F and Cappellaro P 2017 *Rev. Mod. Phys.* **89** 035002
[2] Rong X, Wang M, Geng J, Qin X, Guo M, Jiao M, Xie Y, Wang P, Huang P, Shi F, Cai Y F, Zou C and Du J 2018 *Nat. Commun.* **9** 739
[3] Atature M, Englund D, Vamivakas N, Lee S Y and Wrachtrup J 2018 *Nat. Rev. Mater.* **3** 38
[4] Wang Z Y, Casanova J and Plenio M B 2017 *Nat. Commun.* **8** 14660
[5] Kucsko G, Maurer P C, Yao N Y, Kubo M, Noh H J, Lo P K, Park H and Lukin M D 2013 *Nature* **500** 54
[6] Wang N, Liu G Q, Leong W H, Zeng H L, Feng X, Li S H, Dolde F, Fedder H, Wrachtrup J, Cui X D, Yang S, Li Q and Liu R B 2018 *Phys. Rev. X* **8** 011042
[7] Iwasaki T, Naruki W, Tahara K, Makino T, Kato H, Ogura M, Takeuchi D, Yamasaki S and Hatano M 2017 *ACS Nano* **11** 1238
[8] Nusran N M, Joshi K R, Cho K, Tanatar M A, Meier W R, Bud'ko S L, Canfield P C, Liu Y, Lograsso T A and Prozorov R 2018 *New J. Phys.* **20** 043010
[9] Hanson R and Awschalom D D 2008 *Nature* **453** 1043
[10] Jelezko F, Gaebel T, Popa I, Gruber A and Wrachtrup J 2004 *Phys. Rev. Lett.* **92** 076401
[11] Awschalom D D and Flatté M E 2007 *Nat. Phys.* **3** 153
[12] Zhang N, Yuan H, Zhang C, Xu L X, Zhang J X, Bian G D, Li B and Fang J C 2018 *Appl. Phys. Express* **11** 086602
[13] Zhang C, Yuan H, Zhang N, Xu L X, Li B, Cheng G D, Wang Y, Gui Q and Fang J C 2017 *J. Phys. D: Appl. Phys.* **50** 505104
[14] Weber J R, Koehl W F, Varley J B, Janotti A, Buckley B B, Van de Walle C G and Awschalom D D 2010 *Proc. Natl. Acad. Sci. USA* **107** 8513
[15] Li L, Schroder T, Chen E H, Walsh M, Bayn I, Goldstein J, Gaathon O, Trusheim M E, Lu M, Mower J, Cotlet M, Markham M L, Twitchen D J and Englund D 2015 *Nat. Commun.* **6** 6173
[16] Bian G D, Yuan H, Zhang N, Xu L X, Zhang J X, Fan P C, Wang H L, Zhang C, Shan G C, Zhang Q F and Fang J C 2019 *Appl. Phys. Lett.* **114** 102105
[17] Davidsson J, Ivady V, Armiento R, Ohshima T, Son N T, Gali A and Abrikosov I A 2019 *Appl. Phys. Lett.* **114** 112107
[18] Soykal Ö O, Dev P and Economou S E 2016 *Phys. Rev. B* **93** 081207
[19] de las Casas C F, Christle D J, Ul Hassan J, Ohshima T, Son N T and Awschalom D D 2017 *Appl. Phys. Lett.* **111** 262403
[20] Koehl W F, Buckley B B, Heremans F J, Calusine G and Awschalom D D 2011 *Nature* **479** 84
[21] Wang X P, Zhao M W, Xia H H, Yan S S and Liu X D 2011 *J. Appl. Phys.* **110** 033711
[22] Tu Y, Tang Z, Zhao X G, Chen Y, Zhu Z Q, Chu J H and Fang J C 2013 *Appl. Phys. Lett.* **103** 072103
[23] Wang X P, Zhao M W, Wang Z H, He X J, Xi Y and Yan S S 2012 *Appl. Phys. Lett.* **100** 192401
[24] El Haj Hassan F and Amrani B 2007 *J. Phys. Condens. Matter* **19** 386234
[25] Okuyama H, Kishita Y and Ishibashi A 1998 *Phys. Rev. B* **57** 2257
[26] Kresse G and Hafner J 1993 *Phys. Rev. B* **47** 558
[27] Kresse G and Furthmüller J 1996 *Phys. Rev. B* **54** 11169
[28] Kresse G and Joubert D 1999 *Phys. Rev. B* **59** 1758
[29] Blöchl P E 1994 *Phys. Rev. B* **50** 17953
[30] Perdew J P, Burke K and Ernzerhof M 1996 *Phys. Rev. Lett.* **77** 3865
[31] Monkhorst H J and Pack J D 1976 *Phys. Rev. B* **13** 5188
[32] Deak P, Aradi B, Frauenheim T, Janzen E and Gali A 2010 *Phys. Rev. B* **81** 153203
[33] Heyd J, Scuseria G E and Ernzerhof M 2006 *J. Chem. Phys.* **124** 219906
[34] Van de Walle C G and Neugebauer J 2004 *J. Appl. Phys.* **95** 3851
[35] Gao R X, Bian G D, Yuan H and Wang H L 2021 *J. Phys. D: Appl. Phys.* **54** 505109
[36] Gali A, Fyta M and Kaxiras E 2008 *Phys. Rev. B* **77** 155206
[37] Ivady V, Simon T, Maze J R, Abrikosov I A and Gali A 2014 *Phys. Rev. B* **90** 235205
[38] Gali A 2019 *Nanophotonics* **8** 1907